molecular pharmaceutics

ACS AuthorChoice

Article

pubs.acs.org/molecularpharmaceutics

Terms of Use

Mad2 Checkpoint Gene Silencing Using Epidermal Growth Factor Receptor-Targeted Chitosan Nanoparticles in Non-Small Cell Lung Cancer Model

Ana Vanessa Nascimento,[†,‡] Amit Singh,[§] Hassan Bousbaa,[†,∥] Domingos Ferreira,[‡] Bruno Sarmento,*[,†,⊥] and Mansoor M. Amiji*[,§]

[†]CESPU, Instituto de Investigação e Formação Avançada em Ciências e Tecnologias da Saúde, IINFACTS, Rua Central de Gandra 1317, 4585-116 Gandra PRD, Portugal

[‡]Laboratory of Pharmaceutical Technology, Faculty of Pharmacy, University of Porto, Praça de Gomes Teixeira, 4099-002 Porto, Portugal

[§]Department of Pharmaceutical Sciences, School of Pharmacy, Bouvé College of Health Sciences, Northeastern University, Boston, Massachusetts 02115-5000, United States

[∥]Center of Medicinal Chemistry, University of Porto (CEQUIMED-UP), Praça de Gomes Teixeira, 4099-002 Porto, Portugal

[⊥]INEB−Instituto de Engenharia Biomédica, Rua do Campo Alegre, 4150-180 Porto, Portugal

Supporting Information

ABSTRACT: RNA interference has emerged as a powerful strategy in cancer therapy because it allows silencing of specific genes associated with tumor progression and resistance. Mad2 is an essential mitotic checkpoint component required for accurate chromosome segregation during mitosis, and its complete abolition leads to cell death. We have developed an epidermal growth factor receptor (EGFR)-targeted chitosan system for silencing the *Mad2* gene as a strategy to efficiently induce cell death in EGFR overexpressing human A549 non-small cell lung cancer cells. Control and EGFR-targeted chitosan nanoparticles loaded with small interfering RNAs (siRNAs) against Mad2 were formulated and characterized for size, charge, morphology, and encapsulation efficiency. Qualitative and quantitative intracellular uptake studies by confocal imaging and flow cytometry, respectively, showed time-dependent enhanced and selective intracellular internalization of EGFR-targeted nanoparticles compared to nontargeted system. Targeted nanoparticles showed nearly complete depletion of Mad2 expression in A549 cells contrasting with the partial depletion in the nontargeted system. Accordingly, Mad2-silencing-induced apoptotic cell death was confirmed by cytotoxicity assay and flow cytometry. Our results demonstrate that EGFR-targeted chitosan loaded with *Mad2* siRNAs is a potent delivery system for selective killing of cancer cells.

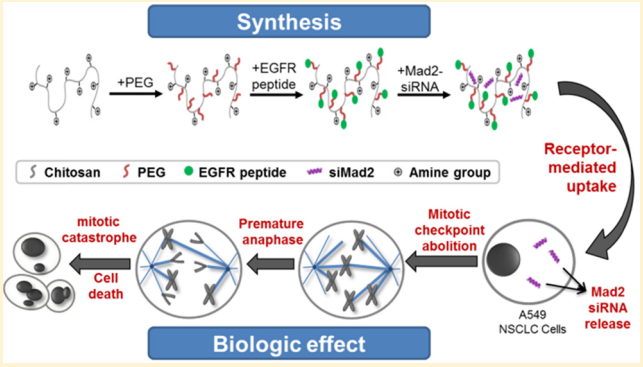

KEYWORDS: *chitosan nanoparticles, epidermal growth factor receptor, Mad2 gene, non-small cell lung cancer, RNA interference, tumor targeting*

INTRODUCTION

Lung cancer is the most common cause of cancer-related deaths worldwide, and non-small cell lung cancer (NSCLC) alone accounts for nearly 80% of the fatalities.[1] One of the major causes of poor clinical outcomes in NSCLC is the development of multidrug resistance and metastatic dissemination to other parts of the body. Refractory disease is the major contributor to the failure of chemotherapy in NSCLC, and it often develops due to poor drug availability, reduced residence time in the tumor, ineffective intracellular penetration, dynamic tumor microenvironment, and other molecular mechanisms adapted by cancer cells.[2,3] An alternative approach to develop new targets to overcome multidrug resistance and augment the therapeutic effects of existing drugs has therefore gained central interest in the scientific community. RNA interference (RNAi) has emerged as a powerful strategy for overcoming drug resistance in NSCLC because it allows silencing of specific genes that could be associated with multidrug resistance.[4] Small interfering ribonucleic acids (siRNAs) allow the possible targeting of vital genes in tumor cells, adapting it to specific tumor types and customizing it to personalized therapy for

Received: April 21, 2014
Revised: September 8, 2014
Accepted: September 11, 2014
Published: September 11, 2014

subtle genotypic and phenotypic variations. Molecular therapy using siRNA has shown great potential in the treatment of diseases such as cancer by silencing crucial genes.[4−6]

The mitotic checkpoint thoroughly ensures that each new cell receives one copy of each chromosome from a dividing cell.[7,8] Many cancer cells have a weaker mitotic checkpoint which accelerates the rate of chromosome losses and gains, thereby acting as a driving force for carcinogenesis.[7,8] However, total suppression of the mitotic checkpoint activity is lethal, thus making it an attractive therapeutic target for siRNA-mediated intervention.[7] In fact, several small molecules targeting the mitotic checkpoint are already under clinical trials. Mad2 is one of the key mitotic checkpoint regulators that sequester Cdc20, thereby inactivating anaphase-promoting complex/cyclosome (APC/C), the complex responsible for triggering anaphase.[8] Mad2 overexpression has been associated with aneuploidy and tumorigenesis and reported in various carcinomas such as liver cancer, breast cancer, soft-tissue sarcoma, B-cell lymphoma, and NSCLC.[9−12] Decreased expression, but not complete obliteration of mitotic checkpoint genes, has been associated with resistance to anti-microtubule drugs and DNA-damaging agents.[13,14] In addition, low levels of Mad2 have been correlated with cisplatin resistance and high levels with sensitivity to the same drug.[15,16] Nonetheless, Mad2 knockdown has been shown to be catastrophic and incompatible with cell viability.[17,18] RNAi-mediated knockdown of Mad2 causes massive chromosome mis-segregation during mitosis, and its null mutation in mice embryos causes early death during embryogenesis.[19] The selectivity and the catastrophic impact of *Mad2* gene silencing on cancer cells, therefore, would be a highly attractive alternative therapy for cancer.

The most challenging obstacle in siRNA therapeutics is their efficient delivery to the target cells. Some of the major difficulties include poor pharmacokinetic properties, enzymatic degradation, cellular permeability restrictions, endosomal trapping, off-target effects, and systemic interferon responses.[20] Careful choice of a suitable delivery vector, however, can aid in circumventing many of these challenges and imparting significant benefit to RNAi as a clinically viable therapeutic option.[21] An ideal delivery vector should fulfill certain criteria before it can be used for therapeutic applications. Biocompatibility, biodegradability, and non-immunogenicity are some of the key consideration while designing a delivery system. We have recently demonstrated hyaluronic acid (HA) derivative-based self-assembling vectors for delivery of siRNA-targeting antiapoptotic genes, *survivin* and *Bcl2*, in the NSCLC tumor model.[22] HA is a natural polymer with a backbone that imparts CD44 receptor-targeting ability to the nanoparticles and could also be used for the synthesis of different derivatives by easy chemical coupling reactions. A detailed in vitro study demonstrated efficient delivery of the payload to the A549 human NSCLC cells and subsequent knockdown of the target gene. In vivo studies in subcutaneous A549 (wild-type, drug-sensitive) and A549−DDP (cisplatin-resistant) NSCLC tumor-bearing mice further demonstrated that this delivery approach could be used in combination with cisplatin to obtain the synergy of antitumor activity and overcome multidrug resistance.[23,24]

Chitosan (CS) is a similar natural polymer that has been extensively studied for nucleic acid delivery in vitro and in vivo.[25−27] CS presents several advantages such as mucoadhesivity, biocompatibility, biodegradability, and low cost of production. Most importantly, chitosan can bind with polyanionic molecules such as DNA or siRNA by electrostatic interaction due to the presence of protonated amine groups in the backbone, leading to the formation of nanosized particles.[28] Besides, the amine backbone of CS allows for chemical modifications such as attachment of poly(ethylene glycol) (PEG) to impart stealth properties or functionalization with ligands to target specific cancer cell types. Although there are no chitosan-based vectors for in vivo administration of nucleic acids at the clinical level, there are numerous publications that report their use as a vaccine adjuvant for oral and intranasal peptide/vaccine delivery.[29−31] Similarly, chitosan has been extensively used as a delivery vector for anticancer therapeutic small molecules and nucleic acids, and therefore, it serves as a promising candidate for siRNA administration in vitro and in vivo.[32,33]

In the present study, we have designed an EGFR-targeted CS vector for delivery of siRNA to selectively silence the *Mad2* gene, thereby depleting the corresponding protein expression and studying its impact in A549 cells. PEG and EGFR-binding peptide derivatives of CS were synthesized, characterized, and used for assembling CS−siMad2 complexes of a size less than 250 nm and a net positive surface charge. In vitro transfection efficiency was evaluated as a function of dose and time, and subsequent silencing activity of the siRNA was confirmed by qRT-PCR at the gene level and flow cytometry at the protein level. Time-dependent cytotoxicity and apoptosis assessments were also carried out to confirm the impact of *Mad2* gene silencing on the cells.

EXPERIMENTAL METHODS

Materials. Two types of chitosan were used in this study. The low molecular weight chitosan (LMW CS) had a viscosity average molecular weight of 50 kDa, and the degree of deacetylation was 75−85%; a higher molecular weight chitosan (HMW CS) had a viscosity average molecular weight of 60−120 kDa, and the degree of deacetylation was 80%. LMW CS and acetic acid glacial were purchased from Sigma-Aldrich Inc. (St. Louis, MO), and HMW CS was a kindly provided by KitoZyme S.A. (Belgium). Fluorescent dye DyLight-488 NHS ester and succinimidyl-([*N*-maleimidopropionamido]ethylene glycol)ester (NHS-PEG-MAL) were purchased from Thermo Scientific (Rockford, IL). Double-stranded siRNAs against Mad2 and nontargeting (NT) siRNA sequence were purchased from Santa Cruz Biotechnology Inc. Amine-reactive Alexa Fluor 488 was purchased from Invitrogen/Life Technologies (Carlsbad, CA), and a Label IT siRNA tracker kit was procured from Mirus Corporation (Madison, WI). Pico-Green fluorescence reagent for quantification of double-stranded nucleic acid constructs was purchased from Invitrogen/Life Technologies (Carlsbad, CA). For Mad2 protein quantification by flow cytometry, the antibody monoclonal anti-Mad2 clone 17D10 was obtained from Sigma (Sigma-Aldrich, St. Louis, MO), and the secondary antibody goat anti-mouse conjugated with Alexa Fluor 568 was from Abcam (Abcam, Cambridge, UK).

Synthesis of Chitosan Derivatives. Both types of chitosan were dissolved in a 2% acetic acid solution at 2 mg/mL and reacted overnight with 10% molar equiv of maleimide−poly(ethylene glycol)−*N*-hydroxysuccinimide (Mal−PEG_{2000}−NHS) to achieve CS−PEG−Mal. The next day, the solution was purified by dialysis (molecular weight cutoff = 10 kDa) in water, and one-half of the amount of chitosan-PEG-Mal was

used for epidermal growth factor receptor (EGFR)-binding peptide modification. This peptide with the following sequence, YHWYGYTPQWVI-, was originally synthesized by Zonghai Li and co-workers and has been demonstrated to be the most efficient in targeting the EGFR receptor.[34] We have extensively used this peptide with inclusion of four glycine spacer terminal cysteine residues to successfully demonstrate its targeting capability in vitro as well as in vivo in various EGFR overexpressing tumor cells.[35−41] The peptide was obtained from Tufts University. A 2-fold molar excess of 17-amino acid EGFR-binding peptide was added to the nanoparticle solution at 4 °C in nitrogen atmosphere overnight to allow the cysteine group of the peptide to react with the maleimide group. The solution was purified by dialysis (molecular weight cutoff = 10 kDa) in water. Glacial acetic acid was added to the dialyzed nanoparticle solution in order to achieve a 5% concentration and then freeze-dried and stored at −20 °C until further use. Nontargeted chitosan derivative was similarly prepared by reaction with $mPEG_{2000}$-NHS followed by acetic acid addition, dialysis, and freeze-drying. The degree of substitution value of PEG on chitosan was estimated by NMR analysis. For each sample, 4 mg of the lyophilized product was dissolved in 0.7 mL of D_2O and characterized by 400 MHz ^1H NMR spectroscopy (Varian, Inc. CA).

Preparation and Characterization of siRNA-Encapsulated Chitosan Nanoparticles. Mad2 and scrambled siRNA duplexes were encapsulated in CS−PEG derivatives in a molar ratio between nitrogen residues from chitosan per nucleic acid phosphate (N/P ratio) of 25/1, 50/1, 75/1, and 100/1 CS−PEG, dissolved in water (1 mg/mL), and siRNA dissolved in nuclease-free water was slowly added under magnetic stirring. The solution was incubated for 30 min at room temperature to facilitate CS−PEG and siRNA complexation and nanoparticle self-assembly prior to use. EGFR-targeted CS−siRNA nanoparticles were prepared using a 1:1 ratio of CS−PEG_{2000}−peptide and $mPEG_{2000}$−CS by the same procedure as described above.

The formed self-assembled nanoparticles were characterized for size, surface charge, morphology, encapsulation efficiency, and stability of the siRNA payload. Particle size, surface charge, and polydispersity index (PDI) of freshly prepared siRNA-loaded chitosan (CS−siRNA) nanoparticles were measured using a ZetaSizer Nano ZS (Malvern Instruments, Worcestershire, UK). Each sample was analyzed in triplicate at 25 °C, and the size and zeta-potential were reported as means ± SD. The encapsulation efficiency was determined using a Quant-iT Pico-Green reagent (Life Technologies, Carlsbad, CA) using a microplate reader (Bio-Tek Instruments, Winooski, VT). A standard curve based on fluorescence emission generated from the binding of Pico-Green to known concentration of double-stranded siRNA was created, and the loading in nanoparticles was determined by subtracting the calculated amount of free siRNA from the initial amount added. Encapsulation efficiency was defined as the ratio percent of siRNA encapsulated in nanoparticles to the total siRNA added.

The morphological characterization of CS−siRNA nanoparticles was carried out under transmission electron microscopy (TEM) using a JEOL JEM-1000 transmission electron microscope (JEOL, Tokyo, Japan). Ten microliters of nanoparticle was dropped on a Formvar-coated copper grid and allowed to stand for 1 min; excess fluid was drained using a Whatman filter paper, and the sample was negatively stained with 1.5% uranyl acetate (1 min) prior to its visualization. The dark staining of siRNA by uranyl acetate offers a high contrast compared to chitosan that can help ascertain the loading of genes in polymeric nanosystems.

Stability of Chitosan−siRNA Nanoparticles. Stability of chitosan−siRNA nanoparticles against RNase digestion was investigated. Chitosan−siRNA nanoparticles in an amount equivalent to 2 μg of siRNA were tested. The nanoparticles were prepared as previously described and in a N/P ratio of 50/1. Each set of particles was in phosphate buffer at pH 7.4 and was subjected to four different conditions: no treatment; incubated for 10 min with 5 μL of heparin (1000 U/mL) for displacing the siRNA from the chitosan nanoparticles; incubated with 4 μL of RNase A (20ug/mL) for 30 min at 37 °C; and incubation with incubation 4 μL of RNase A (20ug/mL) for 30 min at 37 °C followed by heat inactivation of the enzyme and incubation for 10 min with 5 μL of heparin (1000 U/mL). Resulting mixtures were applied to a 4% E-Gel (Invitrogen, Carlsbad, CA), and electrophoresis was carried for 15 min using the E-Gel iBase system. In each gel, free siRNA was applied as a reference. The experiments were performed in triplicate. The resulting gel was imaged on ChemiDoc System (Bio Rad, Waltham, MA) using the software Quantity One.

Cell Culture and Transfection. A549 human lung carcinoma cell lines from the American Type Culture Collection (ATCC, Rockville, MD) were cultured at 37 °C in 5% CO_2 environment in DMEM/F12 medium from Life Technologies (Carlsbad, CA). NIH-3T3 mouse embryo fibroblast cell lines were also purchased from ATCC and cultured in DMEM (Life Technologies, Carlsbad, CA). Both cell culture media were supplemented with 10% fetal bovine serum and 1% penicillin/streptomycin (100 U/mL) (Thermo Fisher Scientific, Waltham, MA). Human pulmonary alveolar epithelial cells (HPAEpiC) were purchased from ScienCell Research Laboratories and cultured in alveolar epithelial cell medium as recommended by the supplier.

Approximately 80 000 cells per well were seeded in a 6-well plate culture for 24 h prior to experiments to achieve approximately 75% confluence for transfection, and the transfection conditions were followed according to the description in Malmo et al.[42] Briefly, fresh nanoparticles were assembled in water as described above and diluted with an equal volume of Opti-MEM (Life Technologies, Carlsbad, CA), supplemented with 270 mM mannitol (Sigma-Aldrich, St. Louis, MO) and 20 mM HEPES (Sigma-Aldrich, St. Louis, MO). Preceding the addition of the nanoparticles, the cells were washed and briefly incubated with Hank's balanced salt solution, HBSS (Life Technologies, Carlsbad, CA), at 37 °C and 5% CO_2. Next, the HBSS solution was removed and the nanoparticles were added to each well. The transfection solution was removed after 6 h of incubation at 37 °C and 5% CO_2 and replaced by regular growth media supplemented with 10% FBS and penicillin/streptomycin (100 U/mL).

Qualitative Analysis of Cellular Trafficking by Confocal Microscopy. Fluorescence confocal microscopy studies were performed in order to assess the qualitative cellular internalization of the nanoparticles. Cells (200 000 cells/well) were seeded on coverslips in 6-well plates and were allowed to attach for 24 h. After incubation for specific periods of time, cells were washed with cold phosphate buffered saline (PBS, pH 7.4), fixed with 4% paraformaldehyde for 20 min, washed with cold PBS, and stained with the fluorescent DNA-binding dye Hoechst 33342 (Invitrogen, Carlsbad, CA) (1 μg/mL) for 5 min. The cells were finally washed with cold PBS, and the

coverslip was inverted on a glass slide in mounting medium. Microscopy images were acquired using an LSM 700 confocal microscope (Carl Zeiss, Gottingen, Germany) equipped with 40× and 63× objectives. For each image, representative focus planes are shown. The images were obtained using a 405 nm (5 mW) laser for Hoechst 33258 (417−477 nm emission), a 488 nm (10 mW) laser for Alexa Fluor 488 labeled chitosan (500−550 nm emission), and a 639 nm (5 mW) laser for Cy5-siMad2 (600−650 nm). Digital images were analyzed using the NIH Image-J software. All setting parameters for fluorescence detection and image analyses were held constant to allow consistency in imaging of the sample for comparison.

Quantitative Cellular Uptake Studies by Flow Cytometry. CS was conjugated with amine-reactive dye Alexa Fluor 488 (Life Technologies, Carlsbad, CA). In order to achieve this modification, the amine-reactive dye Alexa Fluor 488 was dissolved in DMSO (1 mg/mL) and added to an aqueous solution of chitosan (1 mg/mL) and incubated overnight. On the following day, the conjugate was purified by dialysis (molecular weight cutoff = 10 kDa) in PBS pH 7.4 and freeze-dried. Simultaneously, siRNA against Mad2 (siMad2) was labeled with Cy5 dye using the Label IT siRNA tracker kit (Mirus Corporation, Madison, WI) according to the manufacturer's specifications. For flow cytometry, 200 000 cells/well cells were seeded in 6-well plates and left to attach for 24 h. Cells were then transfected with fluorescently labeled siRNA (Cy5-siMad2) encapsulated in Alexa Fluor 488 labeled chitosan. After specific times, the transfection solution was removed, the cells were washed with PBS and prepared for analysis by flow cytometry.

Time-dependent cellular uptake and EGFR targeting of CS−siRNA nanoparticles were quantitatively analyzed using a Becton Dickinson FACS-Calibur 4 Color flow cytometer (BD Biosciences, Franklin Lakes, NJ). The obtained data were analyzed and visualized using the Cell Quest software (BD Biosciences, Franklin Lakes, NJ). After being incubated with nanoparticles for specific time periods, the cells were washed with PBS (Life Technologies, Carlsbad, CA), trypsinized, resuspended in ice-cold PBS supplemented with 5% FBS, and kept on ice until the time of analysis. The relative amounts of intracellular siMad2 were evaluated in the FL-2 channel. The percentage of cellular uptake was calculated on the basis of the geometric mean (Gm) using the following formula:

$$\text{percent uptake} = \frac{(\text{Gm}_{\text{exp}})}{(\text{Gm}_{\text{ctrl}})} \times 100$$

where Gm_{exp} is the Gm of cells in the different experimental conditions and Gm_{ctrl} is the Gm of cells in the control condition, without treatment. The data presented are the mean fluorescent signals from 10 000 events.

Assessment of EGFR-Specific Cellular Internalization. In order to confirm that entry of peptide-modified CS−siRNA nanoparticles into cells is mediated by EGF receptor targeting, competitive inhibition study was performed in A549 cells. The cells were pretreated for 1 h with EGFR-binding peptide (50 μg/mL) prior to exposure with nanoparticle treatment. Simultaneously, the uptake study also used an EGFR non-overexpressing cell line, NIH-3T3. Fluorescently labeled siRNA, purchased from Qiagen (Venlo, The Netherlands), was loaded into chitosan nanoparticles and was incubated with cells for 15 min. Cells were washed with 1× PBS and harvested as described previously for flow cytometric analysis of cellular uptake. The amount of EGFR on A549 and NIH-3T3 was determined by direct immunofluorescence assay via 488 nm labeled EGFR antibody. Briefly, cells from both cell lines were harvested and washed with ice cold PBS, 10% FBS, 1% sodium azide, and resuspended in 3% BSA/PBS solution. The 488 nm labeled EGFR antibody was added to a final concentration of 20 μg/mL. After a 2 h incubation, cells were washed with ice cold PBS, 10% FBS, 1% sodium azide, and resuspended in the same solution followed by flow cytometric analysis.

Determination of In Vitro Gene-Silencing Efficiency. In vitro gene silencing was assessed by qRT-PCR. Cells were transfected with different siMad2 concentrations and incubation periods as described above. At the time of analysis, cells were collected and total RNA was extracted using a GeneJET RNA purification kit (Thermo Scientific, Tewksbury, MA) according to the manufacturer's recommendations. RNA concentration was determined by spectrophotometry using NanoDrop 2000c (Thermo Scientific, Tewksbury, MA). For each sample, 0.5 μg of total RNA was used for cDNA synthesis, and the reverse transcription reaction was performed with a Verso cDNA synthesis kit (Thermo Scientific, Tewksbury, MA) according to the manufacturer's instructions.

Real-time polymerase chain reaction (qPCR) was performed with the LightCycler 480 SYBR Green I Master kit (Roche, Basel, Switzerland), and housekeeping gene glyceraldehyde 3-phosphate dehydrogenase (GAPDH) was used as the endogenous control. The sequences of the primers used in this work were as follows: Mad2 forward (GTGGAACAACTGAAAGATTGGT), Mad2 reverse (GTCACACTCAATATCAAACTGC), GAPDH forward (ACAGTCAGCCGCATCTTC), and GAPDH reverse (GCCCAATACGACCAAATCC). Two microliters of the cDNA was used to evaluate Mad2 expression levels. qPCR steps included a preincubation step for 5 min at 95 °C, followed by 40 cycles of three steps: 10 s at 95 °C, 20 s at 60 °C, and 30 s at 72 °C. The threshold cycle (C_t) values were generated automatically by the LightCycler 480 software, version 1.5, and the comparative method for mRNA level quantification was calculated according to the following formulas:

$$\Delta C_t(\text{treated}) = C_t(\text{target gene in treated}) - C_t(\text{reference gene in treated})$$

$$\Delta C_t(\text{control}) = C_t(\text{target gene in control}) - C_t(\text{reference gene in control})$$

$$\Delta\Delta C_t = \Delta C_t(\text{treated}) - \Delta C_t(\text{control})$$

$$\text{Normalized target gene expression level} = 2^{(-\Delta\Delta Ct)}$$

Normalized target gene expression level = $2^{(-\Delta\Delta C_t)}$, where C_t is the threshold cycle.

Determination of Mad2 Protein Expression Levels by Flow Cytometry. Cell suspensions from different treatments were collected and fixed with 4% formaldehyde for 10 min at room temperature. After being pelleted, the cells were permeabilized with a 0.3% Triton-X solution for 7 min at room temperature. After blocking nonspecific antigens with a PBS solution containing 10% FBS, we incubated the cells for 2 h in the primary antibody solution, 4 μg/mL mouse anti-Mad2 in PBS. After three washing steps with PBS, cells were stained with secondary antibody, anti-mouse conjugated with Alexa

Table 1. Particle Size, Polydispersity Index, Zeta-Potential, and siRNA Encapsulation Efficiency of Chitosan/siRNA Nanoparticles at a NP Ratio of 50

chitosan	chitosan deacetylation degree (%)	size (nm) ± SD	PDI ± SD	zeta-potential (mV) ± SD	encapsulation efficiency (%)
NT-LMW	75−85	106.8 ± 2.1	0.551 ± 0.10	+35.6 ± 3.5	105.1 ± 4
T-LMW	75−85	227.3 ± 1.8	0.362 ± 0.02	+28.3 ± 2.0	99.5 ± 2.4
NT-HMW	78	173.1 ± 1.3	0.672 ± 0.03	+42.8 ± 2.4	101.6 ± 2.3
T-HMW	78	257.1 ± 3.1	0.421 ± 0.01	+13.9 ± 2.9	97.5 ± 3.3

568, in a concentration of 2 μg/mL in PBS for 30 min. After two washing steps, cells were resuspended in 500 μL of PBS and analyzed by flow cytometry.

Cell Viability Analysis. The toxicity of the siRNA-loaded and blank nanoparticles was assessed using the MTT (3-(4,5-dimethylthiazol-2-yl)-2,5-diphenyltetrazolium bromide) assay. Cells were seeded in 96-well plates at a density of 2500 cells/well and were allowed to attach overnight. Then, the cells were washed, and 100 μL of the nanoparticle solution was added to each well (n = 8), incubated at 37 °C for 6 h, and followed by replacement of the solution with complete growth medium. At the specific time points, the medium was renewed with fresh complete medium containing 100 μL of 0.5 mg/mL MTT (Sigma-Aldrich, St. Louis, MO). Two hours after incubation, the medium was replaced by dimethyl sulfoxide (DMSO) to stop the reaction and lyse the cells. Untreated A549 served as a negative control. Absorbance of the solution was measured at 560 nm, and the IC_{50} was calculated using GraphPad Prism software.

RESULTS

Characterization of siRNA-Encapsulated CS Nanoparticles. The grafting of Mal−PEG_{2000}−NHS onto chitosan was confirmed by ^{1}H NMR spectroscopy, and the degree of PEG modification was found to be approximately 10% for both LMW and HMW derivatives (Supporting Information, Figure SI 1). NMR spectra of Mal−PEG_{2000}−NHS show characteristic peaks for methylene protons between 3.5 and 3.7 ppm and a distinct peak at 6.9 for the protons corresponding to the ring protons of the maleimide functional group. The peaks related to the protons on carbon at the α position to the carboxylic group and NHS group are present between 2.5 and 3.0 ppm (Figure SI 1A). The peaks corresponding to protons on the chitosan polymer backbone span between 1.8 and 5.0 ppm, and thus several peaks between PEG and CS overlap in that region (Figure SI 1C). Chitosan derivatives were characterized by a new signal at δ = 2.40 ppm, which was attributed to the oxyethylene group present in the copolymer. The unique peak for the maleimide group at 6.9 from Mal−PEG−NHS and for CS at 2 ppm was used to calculate the total PEG modification on the CS backbone (Figure SI 1D), which was found to be 10%. Further reaction of the PEG−CS derivatives with the EGFR-binding peptide leads to the disappearance of the maleimide peak at 6.9 and the peaks in the range of 6.8−7.3 ppm corresponding to the protons from peptide appears (Figure SI 1B), confirming the successful formation of EGFR-binding peptide-modified PEG−CS for both low (Figure SI 1E) and high (Figure SI 1F) molecular weight CS. NMR analysis could not be used to calculate the exact concentration for EGFR modification on Mal−PEG−CS. However, since the PEG modification was found to be 10% and because the concentration of EGFR-binding peptide used for the grafting to the maleimide group was 2-fold higher, we assume that 100% of maleimide groups were modified.

The mPEG and peptide−PEG derivatives of LMW and HMW CS were complexed with Mad2 siRNA to form the nontargeted (NT-LMW and NT-HMW) and EGFR-targeted (T-LMW and T-HMW) nanoparticles, respectively. We first optimized the siRNA loading efficiency of CS derivatives as a function of N/P ratio. The siRNA loading was found to be nearly 100% for the formulations with N/P ratio of 50/1, 75/1, and 100/1 (Figure SI 2A). However, the subsequent size and charge analysis of these formulations demonstrated that CS−siRNA complexes at a N/P ratio of 50/1 give not only optimum loading but also adequate size (<300 nm) for gene delivery application (Figure SI 2B,C) and were therefore used for all further experiments. The sizes of the four chitosan/siRNA nanoparticles were measured by dynamic light scattering and were found to be in the range of 100−250 nm (Table 1). The nanoparticles formed with LMW CS were characteristically smaller in size compared to those formed using the corresponding HMW CS polymer, suggesting that the polymer chain length plays a role in the size of the nanoparticle assembly. Most importantly, addition of EGFR-binding peptide to the polymer leads to a significant increase in the nanoparticle size. This could be due to the change in the net positive charge of the chitosan, leading to a decrease in the particle packing density, although the ability to bind and encapsulate siRNA remains the same. That indeed appears to be true since the zeta-potential measurement for the NT-LMW nanoparticle was 33.6 ± 3.5 mV, which decreased to 28.3 ± 2 mV for the T-LMW nanoparticles, suggesting a net decrease in positive charge. The zeta-potential of the HMW CS−siRNA nanoparticles also showed a similar trend confirming that peptide modification reduces the net positive charge of CS, thereby affecting its interaction with negatively charged siRNA and rendering a larger size for targeted nanoparticles. The PDI values for the chitosan nanoparticles decreased with the addition of the EGFR peptide for both chitosan molecular weights.

In order to analyze if the change in the net charge of CS leads to a change in siRNA loading efficiency of the targeted formulations, siRNA encapsulation efficiency of all the formulations was assessed. The siRNA loading efficiencies of all the nanoparticle systems were found to be 100% irrespective of the difference in CS composition or molecular weight. This observation confirmed that even though the presence of the peptide affects the assembly of the nanoparticle, it does not have any impact on the loading efficiency and peptide-modified PEG−CS could still encapsulate siRNA efficiently despite the charge compensation.

Transmission electronic microscopy was used to examine the morphologies of the different CS−siRNA nanoparticle formulations (Figure 1). The images of nontargeted CS−siRNA nanoparticles demonstrate a more linear, pendant-like structure, showing a compact packing of CS around the siRNA (Figure 1A,C). The negative stain used for visualization of the particles seems to intercalate in the siRNA to give a dark

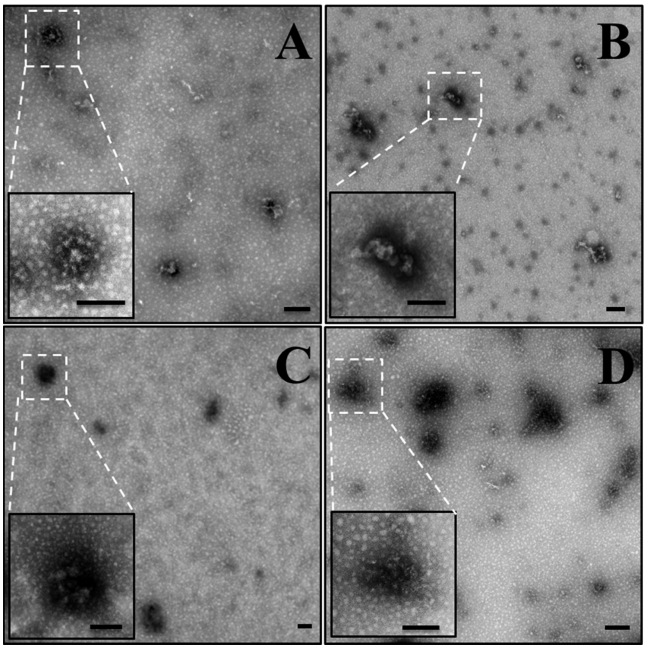

Figure 1. TEM image of chitosan/siRNA nanoparticles at a NP ratio of 50: (A) NT-LMW, (B) T-LMW, (C) NT-HMW, and (D) T-HMW. Scale bar in all images corresponds to 100 nm.

contrast. On the contrary, the targeted nanoparticles with both types of CS complexed to siRNA show larger particle size, confirming the observation made from the DLS measurement (Figure 1B,D). The particle size from the TEM images corresponded well with the size obtained from the DLS measurement for different nanoparticle formulations.

Stability Against RNase Digestion. siRNA degradation is one of the most important barriers for siRNA delivery. Considering that it is associated with loss of activity and therapeutic effect, we have evaluated the protection effect of different siRNA/chitosan derivative complexes against RNase digestion (Figure 2). As expected, free siRNA was degraded completely in the presence of RNase A, while the presence of heparin had no effect on its stability. On the other hand, siRNA, which was incorporated in chitosan particles, remained intact.

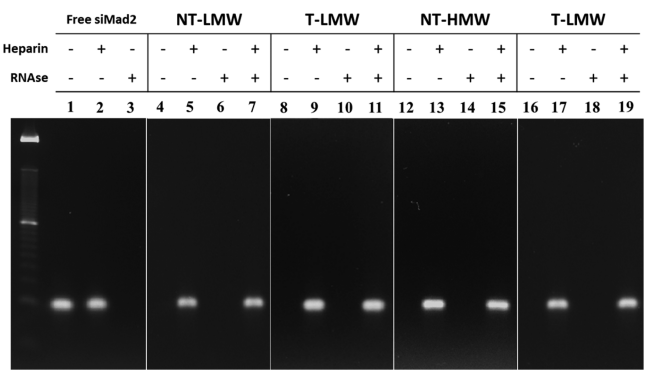

Figure 2. RNase stability of siRNA in the CS/PLA/siRNA complexes. Free siMad2 was a negative control. The complexes were incubated with RNase A (5 mIU/μg siRNA) at 37 °C for 2 h. The reaction was inactivated at 70 °C, and the siRNA was released after incubation for 10 min with 5 μL of heparin (1000 U/mL). Resulting mixtures were analyzed by 4% agarose gel electrophoresis.

This result clearly showed the ability of CS derivatives to protect siRNA from enzymatic degradation.

Qualitative Analysis of Nanoparticle Uptake and Cellular Trafficking. Fluorescence confocal microscopy was employed to visualize the qualitative intracellular uptake of nontargeted and EGFR-targeted CS−siRNA nanoparticles in A549 as a function of time. Intracellular uptake was analyzed at 15, 30, and 60 min for the nontargeted and targeted CS−siRNA nanoparticles at a siRNA concentration of 50 nM. CS was labeled with green fluorescent Alexa Fluor 488, while siMad2 was labeled with red fluorescent Cy5 dye prior to nanoparticle formation. Figure 3 shows the confocal images for

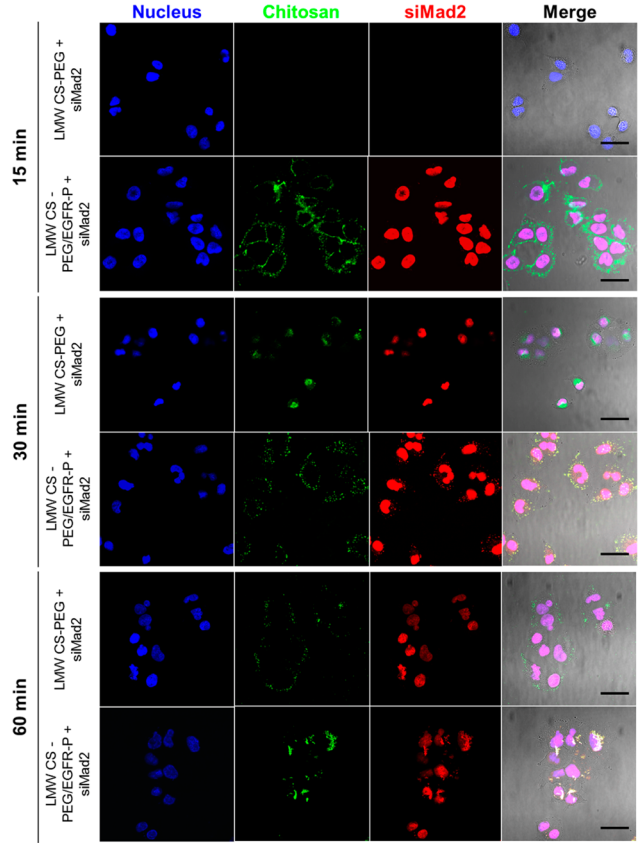

Figure 3. Cell uptake and intracellular trafficking of siMad2-Cy5 encapsulated in chitosan nanoparticles modified with Alexa Fluor 488. Similar results were obtained for 90 kDa chitosan. The concentration of siMad2-Cy5 was 50 nm. Cell nuclei were counterstained with Hoechst 33258 (blue). The column on the right consists on the merge of the fluorescence images and the phase images. Scale bar = 10 μm.

uptake of nontargeted and targeted LMW CS nanoparticles in A549 cells. The images taken after 15 min incubation with the nontargeted and targeted nanoparticles clearly show that, while targeted nanoparticles show internalization, no evident uptake is shown by the nontargeted system. Nontargeted nanoparticles show internalization at 30 min, which confirms that the EGFR-targeting peptide modification of the PEG−CS nanoparticles facilitates an early uptake by receptor-mediated endocytosis. Most importantly, in both cases, green and red fluorescence colocalized on some of the nanoparticles attached to the cellular membrane and inside the cytoplasm, but the majority of red fluorescence (siRNA tag) was rapidly detected in the nucleus. Similar results were also obtained for the nontargeted and targeted HMW CS nanoparticles (data not shown). The

dx.doi.org/10.1021/mp5002894 | Mol. Pharmaceutics 2014, 11, 3515−3527

untreated control cells as well as cell labeled with unlabeled nanoparticle did not show any background autofluorescence (data not shown).

Quantitative Cellular Uptake by Flow Cytometry. In order to ascertain the trend of nanoparticle uptake shown by confocal images and to get a quantitative estimate of intracellular uptake, A549 cells treated with fluorescently labeled nontargeted and targeted nanoparticles in a time-dependent manner were analyzed by flow cytometry. The fluorescence intensity for all of the samples was normalized to the untreated control A549 NSCLC cells. Figure 4 shows the

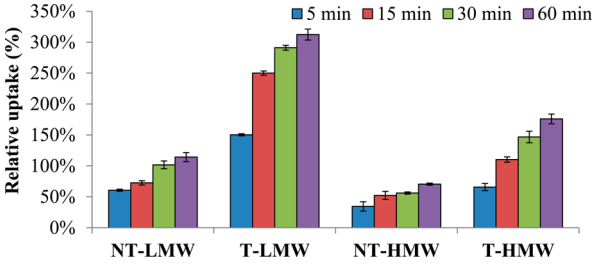

Figure 4. Quantitative relative intracellular uptake study of non-targeted and targeted siRNA-loaded CS nanoparticles by flow cytometry in the A549 cell line. Data are shown as mean ± SD (n = 3).

quantitative relative uptake of Cy5-labeled siRNA as a function of time for the different samples where the T-LMW and T-HMW nanoparticles show significantly higher uptake compared to the respective nontargeted nanoparticles, confirming the trend observed by confocal imaging. Besides, cells show nearly 5-fold increase in fluorescence intensity after 15 min of incubation with NT-LMW and T-LMW nanoparticles, indicating that targeted nanoparticles indeed are rapidly internalized by the cells by receptor-mediated endocytosis and confirmed the much higher uptake shown by confocal imaging. We also analyzed uptake after 5 min of incubation of nanoparticles to see the targeting efficiency of the EGFR-binding peptide, and the results obtained clearly show that T-LMW nanoparticles give better fluorescence intensity after 5 min than NT-LMW nanoparticles after 1 h of incubation. Flow cytometry data also confirmed that LMW CS nanoparticles are more readily internalized by the cells in comparison to the HMW CS nanoparticles. T-LMW nanoparticles show a 312% increase in the relative fluorescence after 60 min on incubation, while the T-HMW nanoparticles show 176% increase in the fluorescent intensity under similar experimental conditions.

Evaluation of Targeted Receptor Internalization. EGF is internalized by ligand-induced receptor-mediated uptake.[43] In order to confirm that higher uptake, better cytotoxicity, and enhanced siRNA efficacy of EGFR-targeted chitosan nanoparticles are due to receptor-mediated endocytosis, the uptake of fluorescently labeled siRNA-containing nanoparticles was evaluated in a series of experiments. One of the strategies adapted was to block the EGFR receptors on the surface of A549 cells by exposing them to excess EGFR-binding peptide. Cells were preincubated with free EGFR-binding peptide for 1 h prior to exposing them to the targeted system, and the nanoparticle uptake was quantitatively determined by FACS (Figure 5). The uptake of the targeted systems significantly decreased when cells were preincubated with free EGFR-binding peptide, suggesting that the targeted nanoparticles show better uptake due to receptor-mediated endocytosis. After

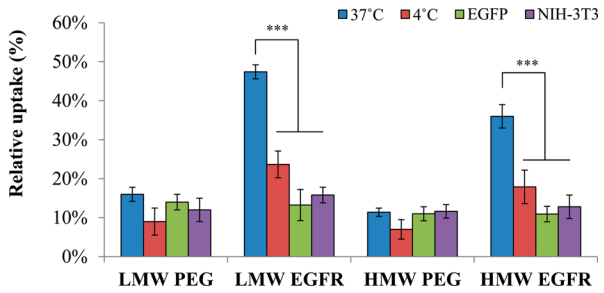

Figure 5. Quantitative relative intracellular uptake study collected by flow cytometry of nontargeted and targeted siRNA-loaded CS nanoparticles in A549 and NIH-3T3 cell lines at 37 and 4 °C and a 50 nM siRNA concentration. Data collected refers to a 15 min incubation period. Data are shown as mean ± SD (n = 3); ***P < 0.001.

15 min of incubation with nanoparticles, A549 showed a decrease in uptake from 47 to 13% for T-LMW and 36 to 11% for T-HMW. Concomitantly, we also studied the uptake of targeted siRNA-loaded nanoparticles in NIH-3T3 fibroblast cells, a low-expressing EGFR-expressing cell line.[44] To determine the expression level of EGFR by A549 and NIH-3T3 cells, the binding of anti-EGFR antibody to the cells was quantified using flow cytometry (Figure SI 3). The variation in the fluorescence intensity of A549 after incubation with anti-EGFR antibody was considerably higher than the variation in NIH-3T3 cells, proving a much higher expression of EGFR on A549 than NIH-3T3 cells. The nanoparticle uptake by NIH-3T3 cells was found to be roughly the same irrespective of the presence or absence of targeting ligand, further cementing that the enhanced uptake of targeted particles in A549 cells is due to the receptor-mediated endocytosis.

Receptor-mediated endocytosis is an energy-dependent process, and so we also performed a nanoparticle uptake study at 4 °C, where receptor-mediated uptake will be the minimum. Indeed, the uptake of targeted systems is dramatically low at 4 °C compared to that when the cells were maintained at 37 °C. Nanoparticle uptake was lower for all treatments at 4 °C; the decrease was, however, statistically significant only in the case of the targeted LMW and HMW nanoparticles. It is also noteworthy that the net uptake upon blocking of the EGFR, using a EGFR non-expressing cell line or performing the study at 4 °C, is the same, indicating conclusively that the presence of EGFR-binding peptide on the nanoparticles facilitates receptor-mediated endocytosis. It is important to understand that these data cannot be compared to the results represented in Figure 4 because the percent labeling of the siRNA was different for that experiment.

Optimization of EGFR Peptide Density on Nanoparticles for Specific Cellular Uptake. The density of the EGFR-binding peptide on the surface could be a key parameter to impact the net uptake of the nanoparticles by the cells. Peptide-modified PEG−CS (10% modification) was blended at 0, 25, 50, 75, and 100% (w/w) to the mPEG-modified CS to vary total peptide content of the nanoparticles and was subsequently tested for uptake in A549 cells as a function of incubation time (Figure SI 4). The cellular uptake profile of nanoparticles with EGFR targeting at 50% or higher concentrations showed almost identical uptake behavior at all time points up to 60 min of incubation. A 50−50 blend of peptide-modified PEG−CS and mPEG-modified CS was,

dx.doi.org/10.1021/mp5002894 | Mol. Pharmaceutics 2014, 11, 3515−3527

therefore, chosen for all subsequent experiments with targeted nanoparticles.

In Vitro *Mad2* Gene Silencing in A459 NSCLC Cells. qRT-PCR was used to evaluate the ability of different formulations to silence the expression of *Mad2* gene in A549 cells. *Mad2*-specific mRNA expression was quantified in a dose- and time-dependent manner after treatment with nontargeted and EGFR-targeted CS nanoparticles. A N/P ratio of 50:1 was used for all of the experiments, and lipofectamine, a cationic lipid transfection reagent-complexed siRNA, was used as a positive control. The dose-dependent gene silencing with varying siRNA concentrations ranging from 5 to 50 nM was tested after 48 h of incubation with cells, as shown in Figure 6A.

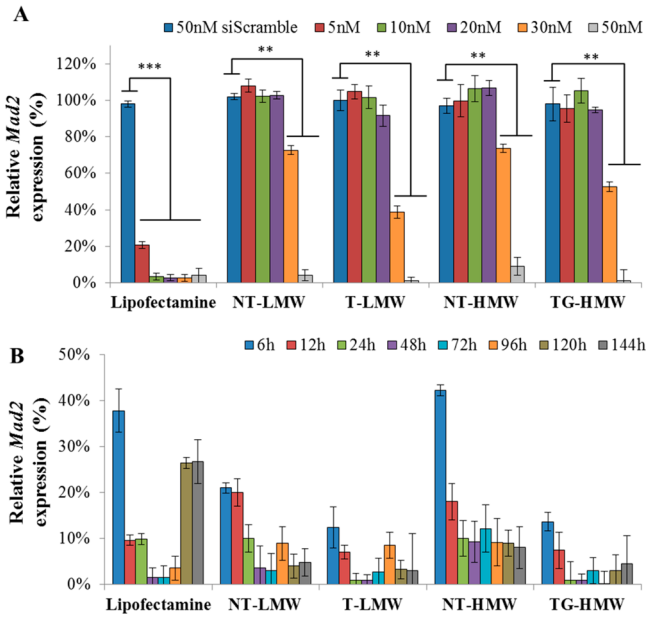

Figure 6. Down-regulation of Mad2 expression by siMad2-loaded nontargeted and targeted CS nanoparticles in the A549 cell line: (A) dose-dependent gene silencing 48 h postdosing and (B) time-dependent gene silencing with 50 nM siMad2 administration. The N/P ratio for all formulations was 50:1. Data are shown as mean ± SD (n = 3); $^{**}P < 0.01$; $^{***}P < 0.001$.

Concentrations below 20 nM did not show a significant change in the *Mad2* expression levels in any of the treatment groups. The gene-silencing effect was significantly improved at 30 nM dose of siRNA, where nontargeted LMW and HMW nanoparticles show 73 ± 2 and 74 ± 7% decreases in the gene expression. However, the silencing effect was more dramatic with EGFR-targeted nanoparticles, which showed 39 ± 6 and 53 ± 4% gene silencing for T-LMW and T-HMW nanoparticles, respectively. *Mad2* expression shows a substantial decrease when the A549 cells were treated with 50 nM of siRNA loaded in CS nanoparticles with 4 ± 2% for NT-LMW, 1 ± 3% for T-LMW, 9 ± 3% for NT-HMW, and 1 ± 2% for T-HMW nanoparticles.

Dose-dependent study showed an efficient gene silencing at 50 nM concentration of siMad2 loaded in all formulations, and therefore, the same concentration was chosen to evaluate a time-dependent gene-silencing profile of the formulation with lipofectamine as the positive control (Figure 6B). Lipofectamine-loaded siMad2 effectively decreases *Mad2* expression level to 10 ± 1% within 12 h of dosing with a significant and sustained silencing efficiency until 96 h. However, the *Mad2* expression level starts to revive at later time points of 120 and 144 h, which could be due to the continued growth and proliferation of nontransfected cells leading to a higher expression level of the gene. On the contrary, treatment with nontargeted and targeted siRNA-loaded CS nanoparticles not only showed an efficient silencing effect at early time points but also showed a sustained silencing effect at the later time periods unlike lipofectamine. *Mad2* expression levels 144 h post-transfection were 5 ± 3, 3 ± 8, 8 ± 5, and 5 ± 6% for NT-LMW, T-LMW, NT-HMW, and T-HMW, respectively. In contrast, lipofectamine-mediated siRNA delivery led to 26 ± 1 and 27 ± 5% expression of the *Mad2* at 120 and 144 h, respectively, indicating that CS nanoparticles serve as a more potent delivery system with an efficient and sustained gene-silencing effect.

Determination of Mad2 Protein Levels in A549 NSCLC Cells. Flow cytometry was used to further investigate the effect of *Mad2* gene silencing on the Mad2 protein level in A549 cells after treatment with CS−siMad2 nanoparticles (Figure 7).

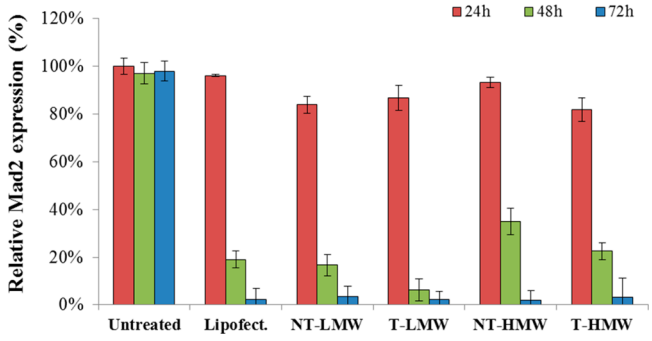

Figure 7. Mad2 protein levels in A549 cells. A549 cells were incubated with 50 nM of siMad2 encapsulated in PEG-modified chitosan nanoparticles and EGFR-targeting peptide-modified chitosan nanoparticles, using a NP ratio in all the cases of 50:1. Data are shown as mean ± SD (n = 3).

A549 cells were exposed to 50 nM of siMad2 loaded in CS nanoparticles, and the protein levels were evaluated up to 72 h post-transfection. The level of Mad2 protein does not show any significant difference after 24 h post-transfection, and the relative protein content was found to be equivalent to the untreated control. Mad2 protein content 48 h post-transfection, however, shows a dramatic decrease in all the cells treated with CS−siMad2 nanoparticles with 19 ± 4, 17 ± 5, 6 ± 2, 35 ± 1, and 23 ± 4% lipofectamine for NT-LMW, T-LMW, NT-HMW, and T-HMW respectively. Incubation for 72 h in different formulations further led to a decrease in the Mad2 protein level, which is consistent with the *Mad2* mRNA expression levels observed by qRT-PCR (Figure 6B).

Cell Viability Analysis with siRNA-Encapsulated CS Nanoparticles. We further conducted cytotoxicity assessment of CS derivatives alone and loaded with siMad2 to study the biocompatibility of the delivery material in A549. MTT assay with different CS derivatives revealed that these derivatives by themselves did not show any apparent toxicity to both the cell lines even after long periods of incubation at the same concentration used for all of the in vitro studies (Figure SI 5). Previous studies have shown that chitosan is an attractive polymer for gene delivery due to several characteristics including its excellent biocompatibility, low toxicity, and low immunogenicity.[45] It has been demonstrated that chitosan only

dx.doi.org/10.1021/mp5002894 | *Mol. Pharmaceutics* 2014, 11, 3515−3527

exhibited significant cytotoxicity at concentrations higher than 0.741 mg/mL, which is 7 times higher than the concentration used in this study.[46] SiMad2-loaded CS nanoparticles on the other hand showed severe cytotoxicity in A549 after 48 h of incubation and kept this trend throughout until 120 h of the study, where the cell viability for all nanoparticles was around 25% (Figure 8A). These results clearly indicate that any

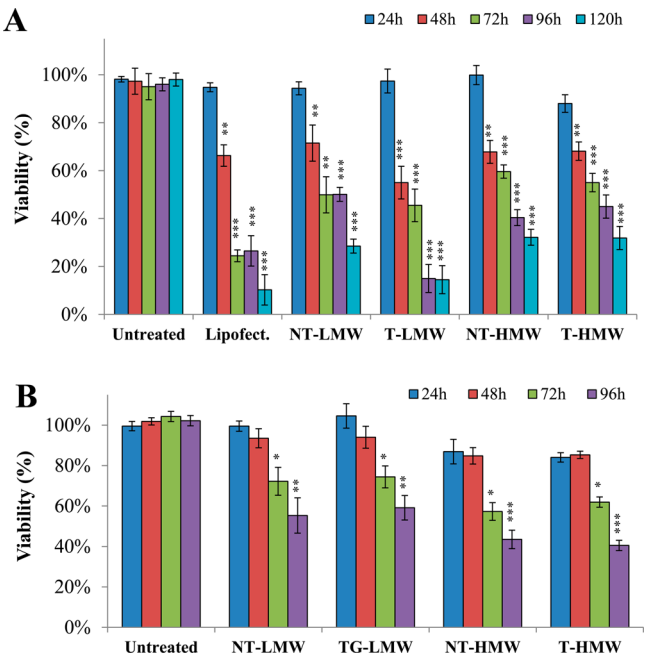

Figure 8. Time-dependent cytotoxicity studies in (A) A549 cells and (B) HPAEpiC upon incubation with 50 nM of siMad2 loaded in CS derivatives. Data are shown as mean ± SD (n = 3); $^{**}P < 0.05$; $^{**}P < 0.01$; $^{***}P < 0.001$.

cytotoxicity effect elicited by the CS nanoparticles is due to the contribution of the siMad2 and that CS derivatives are highly biocompatible and nontoxic. In order to evaluate the cytotoxicity of CS−siMad2 nanoparticles in EGFR non-expressing, noncancerous cells, a human lung primary cell line, HPAEpiC, was used (Figure 8B). All different nanoparticle formulations showed a delayed cytotoxic effect in HPAEpiC when compared to A549 cells. Only after 72 h post-treatment did the chitosan nanoparticles trigger a significant change in HPAEpiC cell viability, while in A549, the effect was visible after 48 h. Interestingly, the cytotoxic effect of the nontargeted and targeted nanoparticles is similar in the primary cells, indicating a similar uptake level, which would be expected because these cells do not overexpress EGFR. Besides, the effect of the treatments was much milder in the primary cells compared to that in the tumor cells at the corresponding incubation periods.

Cellular Apoptosis Studies with siRNA-Encapsulated CS Nanoparticles. In order to evaluate the mechanism of siMad2-induced cell toxicity in A549 cells and confirm that the observed cell death is through an apoptotic pathway, we performed an Annexin V−propidium iodide assay using flow cytometry (Figure 9). Annexin V conjugated to FITC specifically stains phosphatidylserine that translocates from the inner side to the outer surface of the plasma membrane in apoptotic cells. After 48 h post-transfection with T-LMW nanoparticles loaded with siMad2, 58 ± 5% cells exhibited

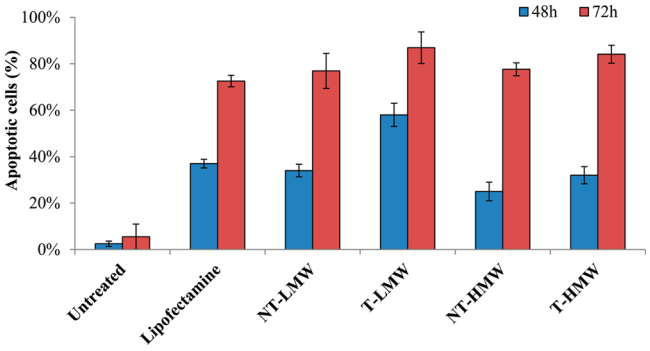

Figure 9. Apoptosis assay using Annexin V−PI staining after exposure of A549 cells to 50 nM siMad2 loaded in CS nanoparticles and lipofectamine as the positive control. Data are shown as mean ± SD (n = 3).

positive Annexin V staining, indicating apoptotic cell population. Treatment with other formulations including lipofectamine shows only 35% apoptotic cell population under similar conditions, which corroborates the cytotoxicity results (Figure 8). The apoptotic cell population increased further after 72 h post-transfection, where T-LMW shows nearly 87 ± 7% Annexin V positive cells while treatment with other formulations showed a lower increase in population. This study ascertains that cytotoxicity mediated by siMad2 administration is due to induction of an apoptotic pathway in the cells.

DISCUSSION

Mad2 protein is a key component of the mitotic checkpoint and a tumor suppressor gene. Its knockdown leads to extensive cell death as a consequence of mitosis failure mainly due to premature mitotic exit.[7,17,18] Therefore, modulating the expression of the *Mad2* gene and subsequently reducing the Mad2 protein translation specifically in cancerous cells could be a promising anticancer strategy. siRNA therapy particularly has shown tremendous promise in selectively down-regulating the activity of a gene of interest.

In order to enhance siRNA delivery specifically for efficient *Mad2* gene silencing in A549 NSCLC cells, we have developed an EGFR-targeted and nontargeted chitosan nanoparticle complex for delivery of siMad2 for application in lung cancer therapy. Cancer cells overexpress several receptors on their surface to increase the uptake of nutrients and growth factors to meet their incessant demand. EGFR is one such surface receptor that has been long known to overexpress on the surface of a majority of cancer tumors and has been intensively studied and characterized in lung cancer.[2,47,48] Human lung adenocarcinoma A549 cells, in particular, have been reported to overexpress the EGFR receptor on their surface and have shown a sensitivity to anti-EGFR therapies.[49] Targeting EGFR therefore serves as a logical approach, and to this end, we derivatized the CS backbone with heterobifunctional PEG to subsequently bind the EGFR-binding peptide, while the nontargeted nanoparticle system was developed using methoxy-PEG modification. The use of EGFR antibody was avoided due to its larger size compared to the EGFR-binding peptide, which often contributes to steric resistance in conjugating to the nanoparticles' surface and also due to its limited diffusion in tissues.[50] Particle size measurement reveals that mPEG-modified nontargeted CS−siMad2 nanocomplexes were in the size range of 100−175 nm depending on the

dx.doi.org/10.1021/mp5002894 | Mol. Pharmaceutics 2014, 11, 3515−3527

molecular weight of the CS, where lower molecular weight CS gives smaller average particle size compared to high molecular weight CS (Table 1). Subsequent EGFR-binding peptide modification of CS prior to complexation with siMad2 leads to an increase in the net average particle size from 106.8 to 227.3 nm for LMW CS and 173.1 to 257.1 nm for HMW CS samples. This increase in the particle size could be attributed to the peptide modification of CS, which leads to a decrease in the net positive charge on the polymer, thereby affecting the complexation with the negatively charged siMad2. Zeta-potential measurement indeed confirms that peptide-modified nanoparticles show a decrease in the net surface charge for both LMW and HMW formulations (Table 1), which would affect the nanoparticle packing in the presence of siRNA even though the encapsulation efficiency remains unaltered as demonstrated by similar siRNA loading profile. CS nanoparticle size upon condensation with siRNA has been studied as a function of the molecular weight of the polymer, and the particle size observed by us is in agreement with that in previously reported literature.[28]

A difference in the nanoparticle size could result in differential uptake characteristics and siRNA release profile, especially since the size difference between nontargeted and targeted LMW CS nanoparticles is dramatically large. In this regard, one would expect a lower intracellular uptake of large-sized particles due to limited diffusion capability.[51] However, on the contrary, all of our experiments suggest that targeted nanoparticles, which are significantly larger, show greater intracellular uptake, suggesting that any size-dependent limitation in uptake is efficiently overcome by targeting the EGFR receptor. Besides, the siRNA efficacy of targeted nanoparticles shows marked improvement over respective nontargeted nanoparticles at all studied time points, indicating that change in nanoparticle size does not affect the siRNA release or activity in any manner.

The siRNA-mediated silencing at gene and protein levels clearly indicated that the EGFR-targeted nanoparticles outperformed their corresponding nontargeted systems and that the LMW CS nanoparticles had better activity than the corresponding HMW CS nanoparticles. As with studying any cell-specific targeted system, it is pertinent to establish that the better activity of targeted nanoparticles is associated with increased intracellular accumulation due to receptor-mediated endocytosis. A series of experiments to study the uptake of the EGFR-targeted system in EGFR non-expressing cells, selective blocking of the receptor by a target peptide, and mitigating receptor-mediated endocytosis by performing the study at 4 °C conclusively proved that the enhanced intracellular uptake and subsequent great siRNA activity shown by the targeted system indeed are a result of EGFR targeting.

Qualitative intracellular uptake studies of all the nanoparticle systems revealed another interesting phenomenon that is usually uncommon with siRNA delivery. Confocal images indicate that the delivery siRNA localizes in the nucleus of the cells especially at later time points, while chitosan remains in the cytoplasm throughout the course of our chosen experimental time points (Figure 3). Such an observation is unusual especially since the RNAi mechanism is known to occur in the cytoplasm where mRNA is mostly found; however, it is not entirely surprising because several other previous studies have reported the same behavior of siRNA.[52,53] It has also been shown that, by diffusion into the nucleus and subsequent export out of the nucleus by Exportin-5, siRNAs can shift between the cytoplasm and the nucleus in a sequence-dependent way.[52−55] The exact mechanism that leads to the localization of siRNA in the nucleus is not well-understood, but it was important to understand whether this property is imparted by the delivery system or is governed by the siRNA itself. To discern this rather intriguing observation further, we repeated the same study with scrambled siRNA, keeping the delivery system unaltered (data not shown), and we did not detect localization of the scrambled siRNA in the nucleus. It is therefore safe to assume that the nuclear localization of siMad2 is not related to the chitosan-based delivery system but is possibly due to the sequence-specific siRNA property.

Several siRNA-loaded delivery vectors are efficiently internalized into the tumor cells but do not show any activity since they fail to escape endosomes and successfully deliver the payload into the cytoplasm. Chitosan as a positively charged biodegradable polymer has been extensively studied specifically for nucleic acid delivery because it can complex with these negatively charged biomolecules.[28] However, several key characteristics of the polymer can influence its in vitro and in vivo performance. Molecular weight of the polymer, for example, can have an impact on the nucleic acid complexation efficiency and subsequent protection. Low molecular weight CS (<10 kDa) shows poor siRNA condensation, whereas intermediate MW CS (<80 kDa) has shown a complete and efficient encapsulation.[56,57] Thus, the MW of CS can greatly impact the size of the nanoparticles (Table 1) as well as the stability of the encapsulated siRNA.[28] We therefore checked the ability of our nanoparticle system to protect the siRNA payload in the presence of RNase, and the studies clearly indicate that the 50 and 90 kDa CS polymers could effectively shield the siRNA from enzymatic activity (Figure 2).

Activity of the siRNA can also be influenced by the choice of CS where delivery using higher molecular weight polymers tends to show better efficacy of the payload.[57] High silencing activity of siMad2 at gene and protein levels affirmed that the CS delivery vector not only protects the payload from degradation but is also able to release them timely to show activity in vitro. However, the molecular weight of the polymer alone cannot entirely govern the nanoparticle performance because our results clearly indicate that the 50 kDa polymer formulation shows better activity compared that of the 90 kDa polymer formulation. Lipofectamine, a commonly used cationic lipid transfection agent, was used as a positive control, which generated a boost effect on gene silencing, but failed to provide a sustained silencing effect over time.[58] CS nanoparticle-mediated delivery, on the other hand, serves as a sustained source of siMad2 in the cells to achieve effective silencing activity for a significantly longer period compared to the positive control (Figure 6). Biological activity of any siRNA is directly related to its release from the carrier, which in turn can be influenced by nanoparticle carrier size, interaction with the payload, stability, etc. It was previously demonstrated that CS molecular weight can impact the biological activity where changing the polymer from 20 to 40 or 80 kDa changed the net activity from 60 to 70%.[57]

Reduction in the level of the Mad2 protein results in premature mitotic exit, multinucleation, and apoptosis-induced cell death.[7,17,18] It was therefore relevant to assess if silencing the *Mad2* gene and subsequent protein expression inflicts any cytotoxic effect on the cells. A time-dependent study with a 50 nM dose of siMad2-loaded CS derivatives in A549 cells demonstrated higher cytotoxicity as a function of increased

incubation time post transfection (Figure 8). All formulations loaded with siMad2 start to show cytotoxic effects around 48 h post-transfection, which correlates extremely well with the Mad2 protein levels in A549 cells with an identical dose of siRNA (Figure 7). Most importantly, blank CS derivatives did not cause any toxicity to the cells (Figure SI 5), thus confirming that the observed cytotoxicity from siMad2-loaded CS nanoparticles is due to siMad2 activity. It has been well-documented that depletion of Mad2 protein level leads to apoptosis-mediated cell death (Figure 9).[17,18]

The human lung primary cell line, HPAEpiC, was used as an example of nontumor human lung primary cell line to evaluate the toxicity profile of the formulation and assess a therapeutic window. The primary alveolar cell line was used to emphasize the two major differences between nontumor cells and the tumor cells: (i) nontumor cells have a much lower proliferation rate. Since the mitotic checkpoint proteins such as Mad2 are only needed during cell division, its abolition would selectively affect proliferating tissues; therefore, cancer cells with high cell proliferation rate would be much more prone to anti-Mad2 therapy compared to their normal counterpart.[7] (ii) EGFR is frequently overexpressed in NSCLC, which would increase the uptake of the EGFR-targeted chitosan nanoparticles when compared with nontumor cells.[59] Due to the absence of EGFR overexpression in the primary cell line, the targeted and nontargeted particles seem to behave in a similar and, in A549 cells, the effect of the targeted particles was more pronounced. This further confirms that the enhanced toxicity demonstrated by the EGFR-targeted nanoparticles is indeed due to their targeting effect, which would augment the therapeutic efficacy more effectively in the in vivo setting.

CONCLUSIONS

We have developed an EGFR-targeted chitosan system for silencing the *Mad2* mitotic checkpoint gene in treatment of non-small cell lung cancer. We showed that this system exhibited higher and selective uptake and efficiently knocked down Mad2, resulting in massive cell death by apoptosis. Collectively, our results indicate that the described system can be used as a potential therapeutic strategy for cancer treatment. Further studies are needed to validate these results in vivo.

ASSOCIATED CONTENT

Supporting Information

Additional figures. This material is available free of charge via the Internet at http://pubs.acs.org.

AUTHOR INFORMATION

Corresponding Authors

*B.S. Tel: +351 226074900/82. Fax: +351 226094567. E-mail: bruno.sarmento@ineb.up.pt.

*M.M.A. Tel: 617-373-3137. Fax: 617-373-8886. E-mail: m.amiji@neu.edu.

Notes

The authors declare no competing financial interest.

ACKNOWLEDGMENTS

This study was supported by the National Cancer Institute's Alliance for Nanotechnology in Cancer Nanotechnology Platform Partnership (CNPP) Grant U01-CA151452. A.V.N. is a Visiting Scholar supported by the Portuguese Government, FCT grant (Grant No. SFRH/BD/69271/2010). We also thank to CESPU−Cooperativa de Ensino Superior Politécnico e Universitário (Grant No. 02-GCQF-CICS-2011N), from the European Regional Development Fund (ERDF) through the Programa Operacional Factores de Competitividade (COMPETE), to Portuguese funds through FCT in the framework of the project PEst-C/SAU/LA0002/2013, and co-financed by North Portugal Regional Operational Programme (ON.2 − O Novo Norte) in the framework of project SAESCTN-PIIC&DT/2011, under the National Strategic Reference Framework (NSRF).

ABBREVIATIONS

CS, chitosan; CS NPs, chitosan nanoparticles; LMW, low molecular weight; HMW, high molecular weight; NT, non-targeting; NSCLC, non-small cell lung cancer; RNAi, RNA interference; Mad2, mitotic arrest deficient 2; APC/C, anaphase-promoting complex/cyclosome; siRNAs, small interfering ribonucleic acids; N/P, amine/phosphate; Gm, geometric mean

REFERENCES

(1) Zhao, Y.; Lu, H.; Yan, A.; Yang, Y.; Meng, Q.; Sun, L.; Pang, H.; Li, C.; Dong, X.; Cai, L. ABCC3 as a marker for multidrug resistance in non-small cell lung cancer. *Sci. Rep.* **2013**, *3*, 3120.

(2) Nascimento, A. V.; Bousbaa, H.; Ferreira, D.; Sarmento, B. Non-small cell lung carcinoma: an overview on targeted therapy. *Curr. Drug Targets* **2014**, PMID 24875380.

(3) Saad, M.; Garbuzenko, O. B.; Minko, T. Co-delivery of siRNA and an anticancer drug for treatment of multidrug-resistant cancer. *Nanomedicine* **2008**, *3*, 761−776.

(4) Ashihara, E.; Kawata, E.; Maekawa, T. Future prospect of RNA interference for cancer therapies. *Curr. Drug Targets* **2010**, *11*, 345−360.

(5) Bora, R. S.; Gupta, D.; Mukkur, T. K.; Saini, K. S. RNA interference therapeutics for cancer: challenges and opportunities (review). *Mol. Med. Rep.* **2012**, *6*, 9−15.

(6) Kim, D. H.; Rossi, J. J. Strategies for silencing human disease using RNA interference. *Nat. Rev. Genet.* **2007**, *8*, 173−184.

(7) Barbosa, J.; Nascimento, A. V.; Faria, J.; Silva, P.; Bousbaa, H. The spindle assembly checkpoint: perspectives in tumorigenesis and cancer therapy. *Front. Biol.* **2011**, *6*, 147−155.

(8) Silva, P.; Barbosa, J.; Nascimento, A. V.; Faria, J.; Reis, R.; Bousbaa, H. Monitoring the fidelity of mitotic chromosome segregation by the spindle assembly checkpoint. *Cell Proliferation* **2011**, *44*, 391−400.

(9) Sotillo, R.; Hernando, E.; Diaz-Rodriguez, E.; Teruya-Feldstein, J.; Cordon-Cardo, C.; Lowe, S. W.; Benezra, R. Mad2 overexpression promotes aneuploidy and tumorigenesis in mice. *Cancer Cell* **2007**, *11*, 9−23.

(10) Choi, J. W.; Kim, Y.; Lee, J. H.; Kim, Y. S. High expression of spindle assembly checkpoint proteins CDC20 and MAD2 is associated with poor prognosis in urothelial bladder cancer. *Virchows Arch.* **2013**, *463*, 681−687.

(11) Kato, T.; Daigo, Y.; Aragaki, M.; Ishikawa, K.; Sato, M.; Kondo, S.; Kaji, M. Overexpression of MAD2 predicts clinical outcome in primary lung cancer patients. *Lung Cancer* **2011**, *74*, 124−131.

(12) Yu, L.; Liu, S.; Guo, W.; Zhang, B.; Liang, Y.; Feng, Q. Upregulation of Mad2 facilitates in vivo and in vitro osteosarcoma progression. *Oncol. Rep.* **2012**, *28*, 2170−2176.

(13) Furlong, F.; Fitzpatrick, P.; O'Toole, S.; Phelan, S.; McGrogan, B.; Maguire, A.; O'Grady, A.; Gallagher, M.; Prencipe, M.; McGoldrick, A.; McGettigan, P.; Brennan, D.; Sheils, O.; Martin, C.; E, W. K.; O'Leary, J.; McCann, A. Low MAD2 expression levels associate with reduced progression-free survival in patients with high-grade serous epithelial ovarian cancer. *J. Pathol.* **2012**, *226*, 746−755.

(14) Wang, L.; Yin, F.; Du, Y.; Chen, B.; Liang, S.; Zhang, Y.; Du, W.; Wu, K.; Ding, J.; Fan, D. Depression of MAD2 inhibits apoptosis and

increases proliferation and multidrug resistance in gastric cancer cells by regulating the activation of phosphorylated survivin. *Tumour Biol.* **2010**, *31*, 225−232.
(15) Fung, M. K.; Cheung, H. W.; Wong, H. L.; Yuen, H. F.; Ling, M. T.; Chan, K. W.; Wong, Y. C.; Cheung, A. L.; Wang, X. MAD2 expression and its significance in mitotic checkpoint control in testicular germ cell tumour. *Biochim. Biophys. Acta* **2007**, *1773*, 821−832.
(16) Cheung, H. W.; Jin, D. Y.; Ling, M. T.; Wong, Y. C.; Wang, Q.; Tsao, S. W.; Wang, X. Mitotic arrest deficient 2 expression induces chemosensitization to a DNA-damaging agent, cisplatin, in nasopharyngeal carcinoma cells. *Cancer Res.* **2005**, *65*, 1450−1458.
(17) Michel, L. S.; Liberal, V.; Chatterjee, A.; Kirchwegger, R.; Pasche, B.; Gerald, W.; Dobles, M.; Sorger, P. K.; Murty, V. V.; Benezra, R. MAD2 haplo-insufficiency causes premature anaphase and chromosome instability in mammalian cells. *Nature* **2001**, *409*, 355−359.
(18) Michel, L.; Diaz-Rodriguez, E.; Narayan, G.; Hernando, E.; Murty, V. V.; Benezra, R. Complete loss of the tumor suppressor MAD2 causes premature cyclin B degradation and mitotic failure in human somatic cells. *Proc. Natl. Acad. Sci. U.S.A.* **2004**, *101*, 4459−4464.
(19) Manchado, E.; Guillamot, M.; Malumbres, M. Killing cells by targeting mitosis. *Cell Death Differ.* **2012**, *19*, 369−377.
(20) Burnett, J. C.; Rossi, J. J. RNA-based therapeutics: current progress and future prospects. *Chem. Biol.* **2012**, *19*, 60−71.
(21) Aigner, A. Applications of RNA interference: current state and prospects for siRNA-based strategies in vivo. *Appl. Microbiol. Biotechnol.* **2007**, *76*, 9−21.
(22) Ganesh, S.; Iyer, A. K.; Morrissey, D. V.; Amiji, M. M. Hyaluronic acid based self-assembling nanosystems for CD44 target mediated siRNA delivery to solid tumors. *Biomaterials* **2013**, *34*, 3489−3502.
(23) Ganesh, S.; Iyer, A. K.; Gattacceca, F.; Morrissey, D. V.; Amiji, M. M. In vivo biodistribution of siRNA and cisplatin administered using CD44-targeted hyaluronic acid nanoparticles. *J. Controlled Release* **2013**, *172*, 699−706.
(24) Ganesh, S.; Iyer, A. K.; Weiler, J.; Morrissey, D. V.; Amiji, M. M. Combination of siRNA-directed gene silencing with cisplatin reverses drug resistance in human non-small cell lung cancer. *Mol. Ther.* **2013**, *2*, e110.
(25) Jean, M.; Alameh, M.; De Jesus, D.; Thibault, M.; Lavertu, M.; Darras, V.; Nelea, M.; Buschmann, M. D.; Merzouki, A. Chitosan-based therapeutic nanoparticles for combination gene therapy and gene silencing of in vitro cell lines relevant to type 2 diabetes. *Eur. J. Pharm. Sci.* **2012**, *45*, 138−149.
(26) Lai, W. F.; Lin, M. C. Nucleic acid delivery with chitosan and its derivatives. *J. Controlled Release* **2009**, *134*, 158−168.
(27) Jean, M.; Smaoui, F.; Lavertu, M.; Methot, S.; Bouhdoud, L.; Buschmann, M. D.; Merzouki, A. Chitosan-plasmid nanoparticle formulations for IM and SC delivery of recombinant FGF-2 and PDGF-BB or generation of antibodies. *Gene Ther.* **2009**, *16*, 1097−1110.
(28) Ragelle, H.; Vandermeulen, G.; Preat, V. Chitosan-based siRNA delivery systems. *J. Controlled Release* **2013**, *172*, 207−218.
(29) Koppolu, B. P.; Smith, S. G.; Ravindranathan, S.; Jayanthi, S.; Suresh Kumar, T. K.; Zaharoff, D. A. Controlling chitosan-based encapsulation for protein and vaccine delivery. *Biomaterials* **2014**, *35*, 4382−4389.
(30) Scherliess, R.; Buske, S.; Young, K.; Weber, B.; Rades, T.; Hook, S. In vivo evaluation of chitosan as an adjuvant in subcutaneous vaccine formulations. *Vaccine* **2013**, *31*, 4812−4819.
(31) Andrade, F.; Antunes, F.; Nascimento, A. V.; da Silva, S. B.; das Neves, J.; Ferreira, D.; Sarmento, B. Chitosan formulations as carriers for therapeutic proteins. *Curr. Drug Discovery Technol.* **2011**, *8*, 157−172.
(32) Agnihotri, S. A.; Mallikarjuna, N. N.; Aminabhavi, T. M. Recent advances on chitosan-based micro- and nanoparticles in drug delivery. *J. Controlled Release* **2004**, *100*, 5−28.
(33) Park, J. H.; Saravanakumar, G.; Kim, K.; Kwon, I. C. Targeted delivery of low molecular drugs using chitosan and its derivatives. *Adv. Drug Delivery Rev.* **2010**, *62*, 28−41.
(34) Schafer, A.; Pahnke, A.; Schaffert, D.; van Weerden, W. M.; de Ridder, C. M.; Rodl, W.; Vetter, A.; Spitzweg, C.; Kraaij, R.; Wagner, E.; Ogris, M. Disconnecting the yin and yang relation of epidermal growth factor receptor (EGFR)-mediated delivery: a fully synthetic, EGFR-targeted gene transfer system avoiding receptor activation. *Human Gene Ther.* **2011**, *22*, 1463−1473.
(35) Milane, L.; Duan, Z. F.; Amiji, M. Pharmacokinetics and biodistribution of lonidamine/paclitaxel loaded, EGFR-targeted nanoparticles in an orthotopic animal model of multi-drug resistant breast cancer. *Nanomedicine* **2011**, *7*, 435−444.
(36) Milane, L.; Duan, Z.; Amiji, M. Development of EGFR-targeted polymer blend nanocarriers for combination paclitaxel/lonidamine delivery to treat multi-drug resistance in human breast and ovarian tumor cells. *Mol. Pharmaceutics* **2011**, *8*, 185−203.
(37) Xu, J.; Singh, A.; Amiji, M. M. Redox-responsive targeted gelatin nanoparticles for delivery of combination wt-p53 expressing plasmid DNA and gemcitabine in the treatment of pancreatic cancer. *BMC Cancer* **2014**, *14*, 75.
(38) Ganta, S.; Singh, A.; Patel, N. R.; Cacaccio, J.; Rawal, Y. H.; Davis, B. J.; Amiji, M. M.; Coleman, T. P. Development of EGFR-targeted nanoemulsion for imaging and novel platinum therapy of ovarian cancer. *Pharm. Res.* **2014**, PMID: 24643932.
(39) Milane, L.; Duan, Z.; Amiji, M. Therapeutic efficacy and safety of paclitaxel/lonidamine loaded EGFR-targeted nanoparticles for the treatment of multi-drug resistant cancer. *PLoS One* **2011**, *6*, e24075.
(40) Xu, J.; Gattacceca, F.; Amiji, M. Biodistribution and pharmacokinetics of EGFR-targeted thiolated gelatin nanoparticles following systemic administration in pancreatic tumor-bearing mice. *Mol. Pharmaceutics* **2013**, *10*, 2031−2044.
(41) Li, Z.; Zhao, R.; Wu, X.; Sun, Y.; Yao, M.; Li, J.; Xu, Y.; Gu, J. Identification and characterization of a novel peptide ligand of epidermal growth factor receptor for targeted delivery of therapeutics. *FASEB J.* **2005**, *19*, 1978−1985.
(42) Malmo, J.; Sandvig, A.; Varum, K. M.; Strand, S. P. Nanoparticle mediated P-glycoprotein silencing for improved drug delivery across the blood-brain barrier: a siRNA-chitosan approach. *PLoS One* **2013**, *8*, e54182.
(43) Fan, Z.; Lu, Y.; Wu, X.; Mendelsohn, J. Antibody-induced epidermal growth factor receptor dimerization mediates inhibition of autocrine proliferation of A431 squamous carcinoma cells. *J. Biol. Chem.* **1994**, *269*, 27595−27602.
(44) Maya, S.; Sarmento, B.; Lakshmanan, V. K.; Menon, D.; Seabra, V.; Jayakumar, R. Chitosan cross-linked docetaxel loaded EGF receptor targeted nanoparticles for lung cancer cells. *Int. J. Biol. Macromol.* **2014**, *69*, 532−541.
(45) Howard, K. A.; Rahbek, U. L.; Liu, X.; Damgaard, C. K.; Glud, S. Z.; Andersen, M. O.; Hovgaard, M. B.; Schmitz, A.; Nyengaard, J. R.; Besenbacher, F.; Kjems, J. RNA interference in vitro and in vivo using a novel chitosan/siRNA nanoparticle system. *Mol. Ther.* **2006**, *14*, 476−484.
(46) Huang, M.; Khor, E.; Lim, L. Y. Uptake and cytotoxicity of chitosan molecules and nanoparticles: effects of molecular weight and degree of deacetylation. *Pharm. Res.* **2004**, *21*, 344−353.
(47) Hirsch, F. R.; Scagliotti, G. V.; Langer, C. J.; Varella-Garcia, M.; Franklin, W. A. Epidermal growth factor family of receptors in preneoplasia and lung cancer: perspectives for targeted therapies. *Lung Cancer* **2003**, *41*, S29−S42.
(48) Scagliotti, G. V.; Selvaggi, G.; Novello, S.; Hirsch, F. R. The biology of epidermal growth factor receptor in lung cancer. *Clin. Cancer Res.* **2004**, *10*, 4227s−4232s.
(49) Kurai, J.; Chikumi, H.; Hashimoto, K.; Yamaguchi, K.; Yamasaki, A.; Sako, T.; Touge, H.; Makino, H.; Takata, M.; Miyata, M.; Nakamoto, M.; Burioka, N.; Shimizu, E. Antibody-dependent cellular cytotoxicity mediated by cetuximab against lung cancer cell lines. *Clin. Cancer Res.* **2007**, *13*, 1552−1561.

(50) Proske, D.; Blank, M.; Buhmann, R.; Resch, A. Aptamers—basic research, drug development, and clinical applications. *Appl. Microbiol. Biotechnol.* **2005**, *69*, 367−374.
(51) Prabha, S.; Zhou, W. Z.; Panyam, J.; Labhasetwar, V. Size-dependency of nanoparticle-mediated gene transfection: studies with fractionated nanoparticles. *Int. J. Pharm.* **2002**, *244*, 105−115.
(52) Langlois, M. A.; Boniface, C.; Wang, G.; Alluin, J.; Salvaterra, P. M.; Puymirat, J.; Rossi, J. J.; Lee, N. S. Cytoplasmic and nuclear retained DMPK mRNAs are targets for RNA interference in myotonic dystrophy cells. *J. Biol. Chem.* **2005**, *280*, 16949−16954.
(53) Robb, G. B.; Brown, K. M.; Khurana, J.; Rana, T. M. Specific and potent RNAi in the nucleus of human cells. *Nat. Struct. Mol. Biol.* **2005**, *12*, 133−137.
(54) Berezhna, S. Y.; Supekova, L.; Supek, F.; Schultz, P. G.; Deniz, A. A. siRNA in human cells selectively localizes to target RNA sites. *Proc. Natl. Acad. Sci. U.S.A.* **2006**, *103*, 7682−7687.
(55) Guang, S.; Bochner, A. F.; Pavelec, D. M.; Burkhart, K. B.; Harding, S.; Lachowiec, J.; Kennedy, S. An Argonaute transports siRNAs from the cytoplasm to the nucleus. *Science* **2008**, *321*, 537−541.
(56) Liu, X.; Howard, K. A.; Dong, M.; Andersen, M. O.; Rahbek, U. L.; Johnsen, M. G.; Hansen, O. C.; Besenbacher, F.; Kjems, J. The influence of polymeric properties on chitosan/siRNA nanoparticle formulation and gene silencing. *Biomaterials* **2007**, *28*, 1280−1288.
(57) Fernandes, J. C.; Qiu, X.; Winnik, F. M.; Benderdour, M.; Zhang, X.; Dai, K.; Shi, Q. Low molecular weight chitosan conjugated with folate for siRNA delivery in vitro: optimization studies. *Int. J. Nanomed.* **2012**, *7*, 5833−5845.
(58) Xu, D.; McCarty, D.; Fernandes, A.; Fisher, M.; Samulski, R. J.; Juliano, R. L. Delivery of MDR1 small interfering RNA by self-complementary recombinant adeno-associated virus vector. *Mol. Ther.* **2005**, *11*, 523−530.
(59) Lee, S. M. Is EGFR expression important in non-small cell lung cancer? *Thorax* **2006**, *61*, 98−99.